W. Tyler Brandt[1], Forest Cannon[1], Ava Cooper[1], Luca Delle Monache[1], Kayden Haleakala[2], Benjamin Hatchett[3], Bruce McGurk[4], Ming Pan[1], and F. Martin Ralph[1]

[1] Center for Western Weather and Water Extremes, Scripps Institution of Oceanography, University of California, San Diego, La Jolla, CA, USA.

[2] Department of Civil and Environmental Engineering, University of California, Los Angeles, CA, USA.

[3] Western Regional Climate Center, Desert Research Institute, Reno, CA, USA.

[4] McGurk Hydrologic, Orinda, CA, USA.

Corresponding author: W. Tyler Brandt (wbrandt@ucsd.edu)

Key Points:

- We present two new methods to constrain the elevation of the mountain rain-snow transition.
- Snow pillows detect rain-on-snow as a result of mass perturbations in the snow water equivalent induced by heavy rainfall.
- Remotely sensed snow grain size identifies the extent of the end-of-storm rain-snow transition when rain occurs on snow.

Abstract

The elevation of the mountain rain-snow transition is critical for short-term hazard forecasting and longer-term water supply considerations. Despite the transition's importance, direct in-situ observations are rare. Here we present two new methods that utilize "anomalous" snow observations to detect rainfall during rain-on-snow: (1) a mass fluctuation at snow pillow sites, and (2) inflated remotely sensed snow grain sizes. Using auxiliary data, we show snow pillows respond to rain-on-snow with distinct perturbations that appear as pulses, collapses and declines within the snow water equivalent. We use these responses to identify mountain-scale rain-snow transitions across California's Sierra Nevada. We also show how a threshold approach (>200 m) for remotely sensed snow grain size can identify rain-on-snow as snow grain sizes artificially inflate due to a liquid water film. While the methods are not predictive, if paired retroactively with hydrometeorological models, these new methods have the potential to improve predictive streamflow capabilities.

Plain Language Summary

Where is it raining or snowing? The question is essential to water managers making decisions in mountain environments during precipitation events with high rain-snow transitions for flood mitigation. However, despite its importance, the rain-snow transition is still largely an unknown. Measuring the elevation of this transition is difficult—particularly across mountainous terrain with extremes in elevation, slopes, vegetation and a lack of line power. Here we document

two new approaches that utilize existing technology. First, we show how snow pillows respond under heavy rain-on-snow (ROS), enabling rainfall detection. And second, we show how satellite estimates of the snow grain size can be used to detect the rain-snow transition, thereby filling the spatial "gaps" between snow pillows. Taken together, these new tools improve our ability to resolve the rain-snow transition across mountain environments. While retroactive, the new measures will enhance our ability to model extreme precipitation events facilitating better future streamflow and flood forecasting.

1 Introduction

In temperate montane environments worldwide, the elevation of the rain-snow (R-S) transition is critical to building and maintaining a snowpack. The shift from accumulation to ablation begins the runoff season, leading to downstream storage, conveyance, and consumptive use of water during spring and summer seasons. However, climate change is threatening this balance [*Siirila-Woodburn et al.*, 2021]—primarily by increasing the elevation of the R-S transition [*Prein and Heymsfield*, 2020]. This has two key impacts: first, it reduces the snowpack's ability to accumulate and store water [*Dudley et al.*, 2017; *Huss et al.*, 2017; *Knowles et al.*, 2006; *Lynn et al.*, 2020; *Mote et al.*, 2018; *Musselman et al.*, 2018]; and second, it extends the risk of rain-on-snow (ROS) flooding throughout winter in which snowfall typically dominates [*Henn et al.*, 2020a; *Marks et al.*, 1998; *Rössler et al.*, 2014].

Climate change aside, montane ROS is not an unusual phenomenon due to within-event increases in the R-S transition. These events only become problematic when: (1) large rainfall intensities exceed the snow's water-holding capacity, generating runoff from typically snowfall-dominated areas [*Rössler et al.*, 2014; *Würzer et al.*, 2016]; or (2) when the aforementioned conditions are supplemented with snowmelt enhanced by, for example, downwelling longwave radiation, and/or the turbulent fluxes [*Li et al.*, 2019; *Marks et al.*, 1998; *Mazurkiewicz et al.*, 2008; *Pomeroy et al.*, 2016]. In California's Sierra Nevada—the study site for this paper—often catchment-wide rainfall, and not snowmelt, tends to drive much of the runoff response for ROS floods [*Kattelmann*, 1997; *Wayand et al.*, 2015].

ROS floods are conceptually quite simple—a high R-S transition leads to ROS that generates a runoff response. However, these events are extraordinary hard to forecast and parse (i.e., which component drove the runoff response) due to a host of atmospheric and land-based physics that vary in both space and time. The necessary "ingredients" include: the elevation of the R-S transition; the rainfall intensity; the snow water equivalent (SWE); the snowpack's cold content, liquid water content and stratigraphy; and the snowpack's energy balance throughout the storm. While we can observe many of these variables continuously, doing so for a single event, let alone a series of events and across space, is cost-prohibitive and sometimes dangerous for field personnel. Nonetheless, we can constrain the problem by leveraging state-of-the-science atmospheric models and observations to provide real-time atmospheric forecast information [e.g.,

Hatchett et al., 2020], and we can bookend the snow's condition via airborne platforms like the Airborne Snow Observatory [*Brandt et al.*, 2020; *Painter et al.*, 2016].

Despite these innovations, important knowledge gaps remain—one of the most critical is also the most basic: confirmation of where is it raining, snowing, or a mix of both [*Henn et al.*, 2020b; *Sumargo et al.*, 2020]. Utilizing a unique and extensive network of vertically profiling radars upwind of California's Sierra Nevada, *Henn et al.* [2020b] demonstrated that while the mean bias between the observed R-S transition and atmospheric forecast models is relatively low across a range of forecast lead times (200 m), the error increases rapidly with larger lead times (700-800m). However, across all lead times the error is greater still for larger, and warmer storm events. Given that much of the Sierra Nevada's topography can fall within a small elevation range, these relatively small forecasting errors (i.e., even 200 m) has the potential to "consume" the flood pool storage of downstream reservoirs [*Sumargo et al.*, 2020]. Therefore, any refinement of the R-S transition can reduce the risk.

Unfortunately, line power limitations in the mountainous Western US makes direct observation the best "measurement" of the R-S transition [*Harpold et al.*, 2017]. These observations occur at manned stations or from citizen science campaigns [*Arienzo et al.*, 2021]. However, these observations are temporally limited and inconsistent, with mixed phased precipitation producing ambiguous results [*Harpold et al.*, 2017]. Additional methods include: (1) proxies, e.g., air, wet bulb and dew point temperature thresholds, disdrometer measurements of hydrometer size and velocity; (2) coupled observations, e.g., precipitation during snow depth changes; and (3) remotely-sensed observations from ground-based radars and space-based systems (for a full discussion see *Harpold et al.* [2017]). Regardless of the method employed we lack in-situ ground truth observations to validate R-S forecasts.

To address this observation gap, we demonstrate how two existing observational technologies, snow pillows and remote sensing of the snow grain size, can be leveraged to ground truth the R-S transition during ROS. Snow pillows are pressure sensors that measure the overlying mass of water (i.e., the SWE), and changes in mass reflects processes like accumulation, melt, sublimation, wind redistribution, and even snow bridging [*Johnson and Marks*, 2004]. This paper shows how the snow pillow responds to heavy rainfall.

Remote sensing platforms, like the Moderate Resolution Imaging Spectroradiometer (MODIS), retrieve the optical snow grain size through spectral unmixing. *Dozier et al.* [2009] showed snowfall usually reduces the optical grain size, but wet snow inflates the grain size due to a water film inducing grain cluster growth [*Colbeck*, 1979]. Therefore, storms with a relatively high R-S transition (but still below the mountain peak) should exhibit a rapid decrease in the snow grain size with increasing elevation above the R-S transition. Here we establish this remote sensing application and show how it can be used to "fill the gaps" between snow pillows.

2 Study Site and Storm Selection

California's water supply depends on winter storms producing precipitation in the Sierra Nevada [*Catto et al.*, 2012; *Hawcroft et al.*, 2012]. The storms that produce the greatest precipitation totals often feature atmospheric rivers (AR)—which can have dramatic R-S transition elevation variability [*Guan et al.*, 2016; *Hatchett et al.*, 2017; *Ralph et al.*, 2004; *Ralph et al.*, 2020]. Four AR events were selected to investigate the snow pillow ROS response across California's Sierra Nevada. The most recent "cold" AR in late January 2021 acts as a control. The other three ROS events are well-documented. The early February 2017 storm event was the "Oroville Event"—a classic warm AR, described by *White et al.* [2019] and *Henn et al.* [2020a]. The storm in early April 2018 was an exceptionally warm AR that entrained moisture from a typhoon remnant [*Hatchett*, 2018]. Finally, the fourth AR was centered on the 14 February 2019 and became known as the "Valentine's Day Storm" generating precipitation totals exceeding 200 mm with widespread flash flooding, avalanches, and landslides [*Hatchett et al.*, 2020].

3 Data and Methods

All data are presented in UTC.

3.1 Gauges

3.1.1 Snow Pillows

California's Department of Water Resources (DWR) collects data from ~130 stations, which include snow pillows that are part of the Natural Resources Conservation Service (NRCS) Snow Telemetry (SNOTEL) network. We used data from ~95% of available stations (Figure 1; Table S1 for a list and letter codes) with much of the data from California's Sierra Nevada. The data were obtained from DWR's California Data Exchange (CDEC; https://cdec.water.ca.gov/index.html). Snow pillow sites often include temperature and snow depth measurements. While not the focus of this paper, we used this additional data when available to help interpret the snow pillow ROS response. Both SWE and snow depth were manually quality-controlled for spurious values.

3.1.2 Rain Gauge

Rain gauge data (14 stations representing the various watersheds/regions of the snow pillows) were qualitatively used for storm timing. Nevertheless, to minimize snow effects, low-elevation (below ~1500 m) hourly rain gauge data were obtained from CDEC. The elevation threshold is conservative given that the storms of interest had anomalously-high R-S transition elevations (Oroville radar 75^{th} percentile bright band heights for 2017, 2018, and 2019 storms were 2761 m, 3362 m, and 2390 m, respectively—which is considerably higher than median snow level of 1640 m observed at Chico between 2008-2017 [*Hatchett et al.*, 2017]). The data were quality controlled by ensuring that accumulation-season rain gauge totals corresponded to the closest snow pillow peak SWE.

Since rain gauge data were only used qualitatively for storm timing, correction factors for sources of measurement error (e.g., wind effects, and or mixed phased precipitation) were not applied.

3.1.3 Streamflow

Streamflow data (15-minute interval) for two sites were acquired from the U.S. Geological Survey (USGS; https://dashboard.waterdata.usgs.gov/app/nwd/?region=lower48). The data were obtained to provide an integrated measure of the hydrologic response during ROS events. With that in mind, higher-elevation gauges close to the snowline, or above, were selected. Data availability across all measurements lead to the selection of two relatively unimpaired monitoring sites: 11274790 (Tuolumne River at Grand Canyon of Tuolumne above Hetch Hetchy), and 11413000 (North Yuba River Below Goodyears Bar).

3.1.4 Soil Moisture

Error-free co-located DWR soil moisture and snow pillow sites are presently rare in California. However, many of the NRCS SNOTEL sites in the northern Sierra Nevada do have soil moisture measurements. Measurement depths are at: ~50 mm, ~200 mm, and ~500 mm. We used soil moisture data from three NRCS SNOTEL sites to confirm total water input through the snowpack post-snow pillow ROS response. Sites names—ranked from lowest elevation to highest—are: (1) Tahoe City Cross (NRCS SNOTEL: 809) at 2072 m; (2) Palisades Tahoe (NCRS SNOTEL: 784) at 2442 m; and (3) Mt Rose Ski Area (NRCS SNOTEL: 652) at 2683 m. NRCS SNOTEL data can be obtained from: https://wcc.sc.egov.usda.gov/reportGenerator/.

3.2 Remote Sensing

3.2.1 Snow Level Radars

Melt elevations from six Frequency Modulated-Continuous Wave (FMCW) snow level radars within California's Central Valley were obtained from the National Oceanic and Atmospheric Administration (NOAA) physical sciences website (https://psl.noaa.gov/data/obs/datadisplay/). California has a unique network of these radars deployed through a partnership between DWR and the NOAA/Hydrometeorology Testbed to monitor ARs [*White et al.*, 2013]. Stations used herein include Shasta Dam (STD), Oroville (OVL), Colfax (CFF), New Exchequer (NER), Pine Flat Dam (PFD) and Kernville (KNV). Melting levels (i.e., radar Bright Band Heights (BBH)), for all four storms were retrieved at 10-minute intervals and used to assess the timing of the snow pillow ROS response [*White et al.*, 2010]. Importantly, except for the Eel River snow pillow, all six FMCW radars are "upwind" of the snow pillow sites. Due to snow level bending, the R-S transition may be lower near the mountain crest—ultimately producing a high bias [*Minder and Kingsmill*, 2013; *Mizukami et al.*, 2013]. So, while informative, BBH retrievals are not "ground truth" for the mountain R-S transition.

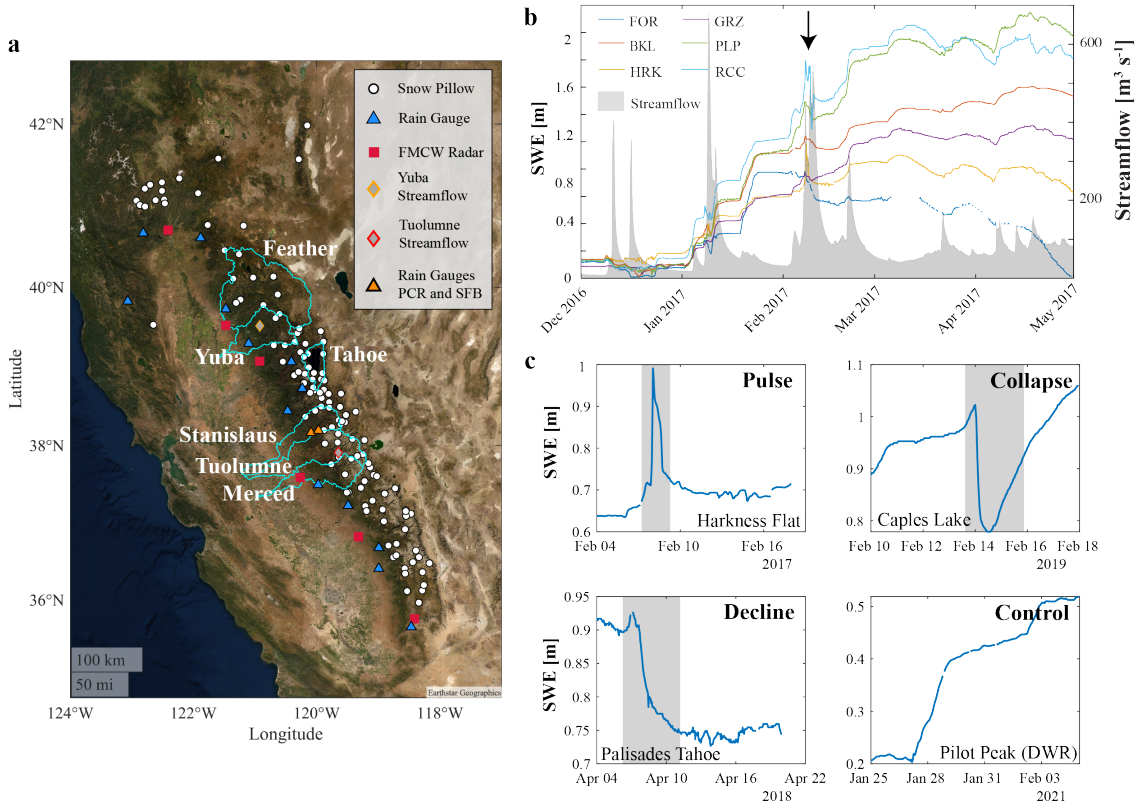

Figure 1. Gauge locations and the snow pillow ROS response. a) a map of gauge locations. b) WY 2017 hourly SWE for snow pillows in the Feather and Yuba basin. Storms appear as smooth, concave increases in SWE. The black arrow demarcates a different "accumulation" signal—that of the snow pillow ROS response. The response occurs simultaneously across all sites, and with large increases in streamflow. c) Variation in the ROS snow pillow perturbation type. The ROS responses have been grouped into three categories: pulses, collapses and declines, although responses can be a blend.

3.2.2 Remotely Sensed Snow Grain Size

We use the MODIS Snow-Covered Area and Grain Size [MODSCAG; *Painter et al.*, 2009] algorithm for snow grain size and fractional snow-covered area (fSCA) estimates. To achieve our stated goals, the remote sensing of the R-S transition is constrained to the following circumstances. First, storms need to conclude with a R-S transition above the event start; otherwise, snowfall at colder temperatures and smaller grain sizes will overlie any inflated grain sizes generated from rain. Second, cloudless imagery needs to bracket the storm—not

always possible during the snow accumulation season. Third, sensor viewing geometry needs to be considered. Despite daily observations of the Earth's surface, MODIS has a 16-day orbital repeat, which necessitates varying sensor viewing geometries that are maximized at = 55°. This stretches nadir pixels (500 m) to 1.003 km by 2.417 km at the swath edges [*Dozier et al.*, 2008]. Therefore, large increases in the viewing geometry when fSCA is small could increase errors. As a result, we carefully selected image days and basins to minimize the zenith angle and constrained the grain size to pixels with a canopy-adjusted fSCA > 30%.

The storms studied herein and their corresponding BBH evolutions dictated that only the 2017 and 2018 storms were suited for grain size remote sensing (Figure S1). In both cases BBHs at the storm-end exceeded the storm-start producing rain in excess of 2,000 m and 3,000 m, respectively. Given the two storm's characteristics, and restrictions due to satellite viewing geometry, we elected to focus this part of the study on the Tuolumne basin (elevation range 0 to 3958 m).

3.3 The Snow Pillow ROS Response

The snow pillow ROS response has been briefly discussed by *Marks et al.* [1998], and *Marks et al.* [2001]. However, to date we are unaware of additional studies. The ROS response becomes apparent when plotting the raw, hourly SWE over the course of a water year (WY; Figure 1b). Responses appear as small "perturbations" from the regular accumulation/ablation pattern, and vary in size, shape and duration. For example, while not studied herein, an additional ROS event is clearly visible in Figure 1b in early January that precedes the February "Oroville Event".

Responses can be parsed into three perturbations: (1) pulses; (2) collapses; and (3) declines (Figure 1c). Although beyond the scope of this paper, we speculate that pulses arise from rain-water drainage through snow, collapses occur due to a sudden loss in pooled liquid within the snow, and declines occur due to rapid snowmelt. Irrespective of the perturbation type, a SWE change of >20 mm was used to register "a response", and features that were present but less than the 20 mm threshold were recorded as a "Hint of ROS". The process was done manually with the help of auxiliary data (i.e., rain gauge timing, BBHs, and snow depth). Automation attempts were made, but ultimately abandoned, due to the variability in shape and size of the perturbations, and other "noises" within the seasonal SWE signal being confounded with the ROS response.

4 Results and Discussion

4.1 Snow Pillow ROS Response

Across storms, the snow pillow ROS responses occur reliably and are corroborated by other measures of the R-S transition (Figure 2). While the responses are temporally correlated, they differ in magnitude and perturbation type (e.g., Figure 1c). But the fact that the responses are concurrent during periods of

otherwise error-free pillow data (Figure 1b), and occur after the initial onset of rain, but prior to the peak of the rising limb of the hydrograph compels us to conclude these perturbations are a response due to ROS rather than sensor error (Figure 2e-h). The only exception is the control during WY2021 in which no streamflow and snow pillow ROS responses were observed, despite two load cell precipitation gauges (SFB: Spring Gap Forebay, and PCR: Pinecrest) registering precipitation, i.e., snowfall was occurring.

Snow pillow ROS responses also occur when BBHs are above the elevation of the snow pillow (Figure 2i-l). The SLI snow pillow is the exception. There are two plausible, physically-based reasons for this: (1) precipitation moisture depletion at higher elevations [*Houze*, 2012; *Kirchner et al.*, 2014; *Roe*, 2005]; and (2) snow level bending [*Minder and Kingsmill*, 2013]. However, just because the snow pillow failed to register a response does not refute the presence of ROS. The availability of snow depth data from both 2017 and 2019 enables a bulk snow density to be estimated. Typically, "cold" storms lower the bulk density; nevertheless, both the 2017 and 2019 storms saw increases in bulk density—a good indicator of ROS (Figure S2). This example illustrates an important point regarding the snow pillow ROS response: for the snow pillow to register any ROS response (even a "hint of ROS"), the mass change in the SWE column above needs to be measurable. Very small amounts of ROS will go unrecorded. We note that this threshold might be different from pillow to pillow depending on their physical lay-out, location and electronics.

Increasing soil moisture is another indication of terrestrial water input from rainfall (Figure S3). During the 2017 storm, lower elevation snow pillows registered ROS responses with soil moisture increases (at all depths). Above the R-S transition, the highest elevation SNOTEL (2,683 m) failed to register a ROS response and any soil moisture increases. However, not all ROS events will produce a soil moisture response as water routing through the snowpack is a nuanced physical process [*Avanzi et al.*, 2019; *Conway and Benedict*, 1994; *Juras et al.*, 2017; *Kattelmann*, 1985; 1987; 1989; *McGurk and Marsh*, 1995; *Singh et al.*, 1997]. For example, lateral overland flow at the snowpack-land surface interface could bypass soil moisture probes entirely [*Eiriksson et al.*, 2013].

Mapping snow pillow ROS responses by perturbation type reveals large scale spatial patterns for the individual storms (Figure 2m-p). During the 2017 storm, there is a north-south, east-west gradient. The northern, lower elevation parts of the Sierra Nevada observed ROS responses. In contrast, the southern and eastern flank of the Sierra Nevada (the highest elevations) accumulated snow. BBHs during the storm suggest that the R-S transition was higher in the southern Sierra Nevada than in the north but cannot produce the same spatial insights that the snow pillow data reveals. Nonetheless, snow pillow ROS responses cannot differentiate the temporal dynamics of a storm in the same way BBHs can—the snow pillow response is akin to a binary: rain, or no rain?

The 2018 storm (unlike the 2017 and 2019 storms) occurred during the ablation season. In many of the snow pillow traces, losses in SWE occurred prior

to the storm indicating saturated conditions. Nonetheless, snow pillow ROS responses were observed in the northern and central Sierra Nevada—many in the mid elevations of the mountain range. Most of them were classified as "declines" with the odd "pulse" prior to the decline. The "decline" perturbation is similar to that observed by *Marks et al.* [1998] during a particularly large ROS event in the Pacific Northwest. Modeling results from that study suggested that the turbulent fluxes were particularly prevalent driving the large reductions in SWE—which we note may have played a similar role during the 2018 storm. Importantly, the 2018 storm proves that the ROS response is not dependent on unsaturated snow conditions; once the irreducible liquid water content has been satisfied, any additional rainfall can still "fill" the available porosity and drain. Like the 2017 storm, the 2019 event exhibited much of the ROS responses in the northern and central Sierra Nevada with a bias towards the lower elevations. However, an assortment of ROS responses was recorded throughout the lower elevations indicating a more spatially heterogenous storm than the event in 2017.

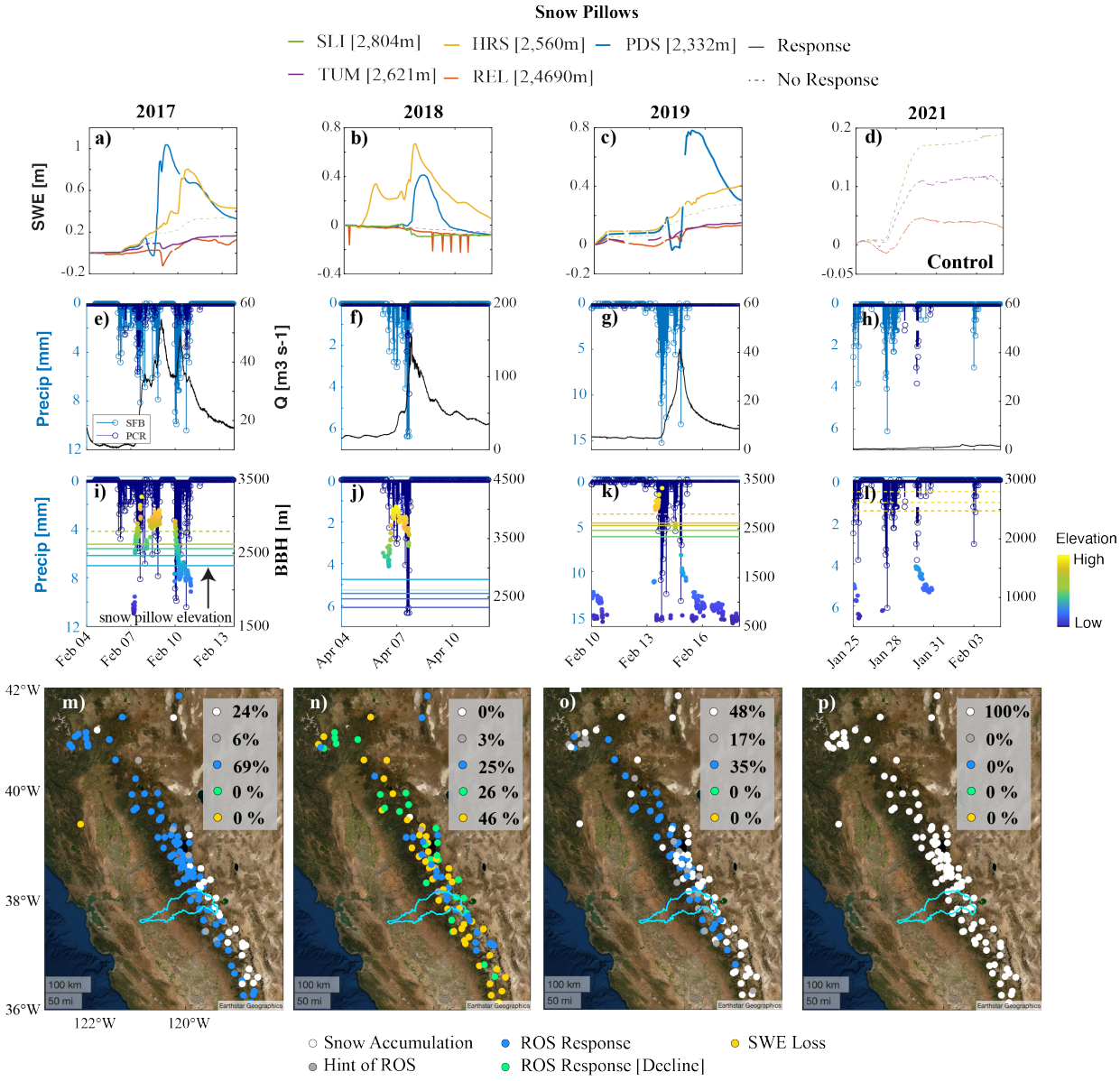

Figure 2. The temporal relationship of the ROS snow pillow response (a-c) as compared with observations of precipitation (e-g), streamflow (e-g), and FMCW radar BBHs (i-k) in the Tuolumne basin. For all three ROS events (2017, 2018, and 2019), snow pillow ROS responses occur simultaneously across sensors, while precipitation is recorded, and streamflow peaks. Most snow pillow ROS responses occur when BBHs are above the elevation of the snow pillow. The snow pillows HRS and PDS respond with larger variations in SWE than the other

snow pillows, more than likely due to snow pillow placement. Both pillows are known to get flooded due to creek outbursts. Even still, the response remains an indicator of ROS. In contrast to the storms in 2017, 2018 and 2019, the "control" storm in 2021 exhibits normal SWE accumulation across all pillows (d), during precipitation (h), and in conjunction with low BBHs (i). Finally, panels (m-o) illustrate the spatial distribution of the ROS response for the Sierra Nevada (the Tuolumne is highlighted in blue) with percentages of total response types. Panel (p) exhibits the control storm in which 100% of snow pillows registered snow accumulation. Note: pulses and collapses were grouped under "ROS Response", whereas declines were left as their own category given their prevalence during the 2018 event.

4.2 Remotely sensed grain size

Remotely sensed grain size was used to map the end-of-storm R-S transition across the Tuolumne and the Sierra Nevada for the storms in 2017 and 2018 (Figure 3). As expected, in both 2017 and 2018, the storms produced smaller grain sizes at high elevations. However, at the lower elevations both storms produced grain sizes of a comparable size, or larger than the pre storm image—unusual behavior for snowfall (Figure 3a and d). From the post storm data in both 2017 and 2018, a rapid shift in the grain size takes place at ~200 m (highlighted in grey in Figures 3a and d). From this observation it follows that grain sizes <200 m indicate snowfall, whilst grain sizes >200 m signify mixed phased precipitation, and/or rain. Across the Sierra Nevada, the grain size threshold matches the snow pillow ROS responses well during the 2017 storm (Figure 3c), and "fills" the gaps between snow pillows greatly enhancing the spatial interpretation of the event. In contrast, the R-S transition of the 2018 event is much higher than the snow pillow network, and the grain size provides valuable insights into the distribution of end-of-storm rainfall at very high elevations.

Using data from the Tuolumne, we tested how well the 200 m threshold (our representation of the R-S transition) matched BBHs at NER (the closest FMCW). For the comparisons, we averaged end of storm BBHs that simultaneously occurred with >1 mm of hourly incremental precipitation at the SFB precipitation gauge. During the 2017 storm the mean BBH was 2,072 m, and grain size estimates (using the median 200 m grain size binned by 100 m elevation bands; Figure 3a) placed the R-S transition slightly higher at 2,158 m—an absolute difference of 86 m. During the 2018 storm, the mean BBH was 3,443 m, and grain size estimates put the R-S transition slightly lower at 3,351 m (figure 3d)—an absolute difference of 92 m. Although not large, the differences between the grain size R-S transition, BBHs, and snow pillow ROS responses can be attributed to the limiting factors for each dataset: BBHs are recorded in the lower Sierra Nevada foothills; the snow pillow ROS response is a single, integrated measure of an event; and the grain size R-S transition is a temporally constrained measurement only sampling a storm at its conclusion. Nevertheless, each of these observations adds insight into the R-S transition and point towards a consistent

conclusion.

One of the primary benefits of the grain size R-S measure is its ability to "gap fill" between stations, or to extend observations beyond the station network (e.g., during the 2018 storm). However, this measure is dependent on both sensor viewing geometry and image timing due to grain metamorphism. We investigated these tradeoffs for the 2017 storm in Figure 3a. The first "predominantly clear sky day" for the Tuolumne post storm was the 11 February (excluding the highest elevations which had clouds). The median zenith angle on 11 February was 37.9°— a large angle indeed. Nonetheless, the zenith angle decreased on the 12 February (35.8°), and again on the 14 February (16.4°; unfortunately, the 13 February image was cloudy). Whilst the zenith angles were arguably more appropriate on the 14 February, the grain sizes post storm rapidly increased between dates (Figure 3a). Based on the findings of *Dozier et al.* [2008] (namely that grain sizes should be minimized post storm), we argue that the grain sizes on the 11 and 12 February actually appear realistic and appropriate for the R-S transition despite the suboptimal viewing geometry (note, we used imagery from the 12 February in Figure 4b and 4c due to some partial cloud cover on the 11 February). We emphasize that the grain size technique is case-specific, and any future investigations should apply the same level of "healthy skepticism" used herein.

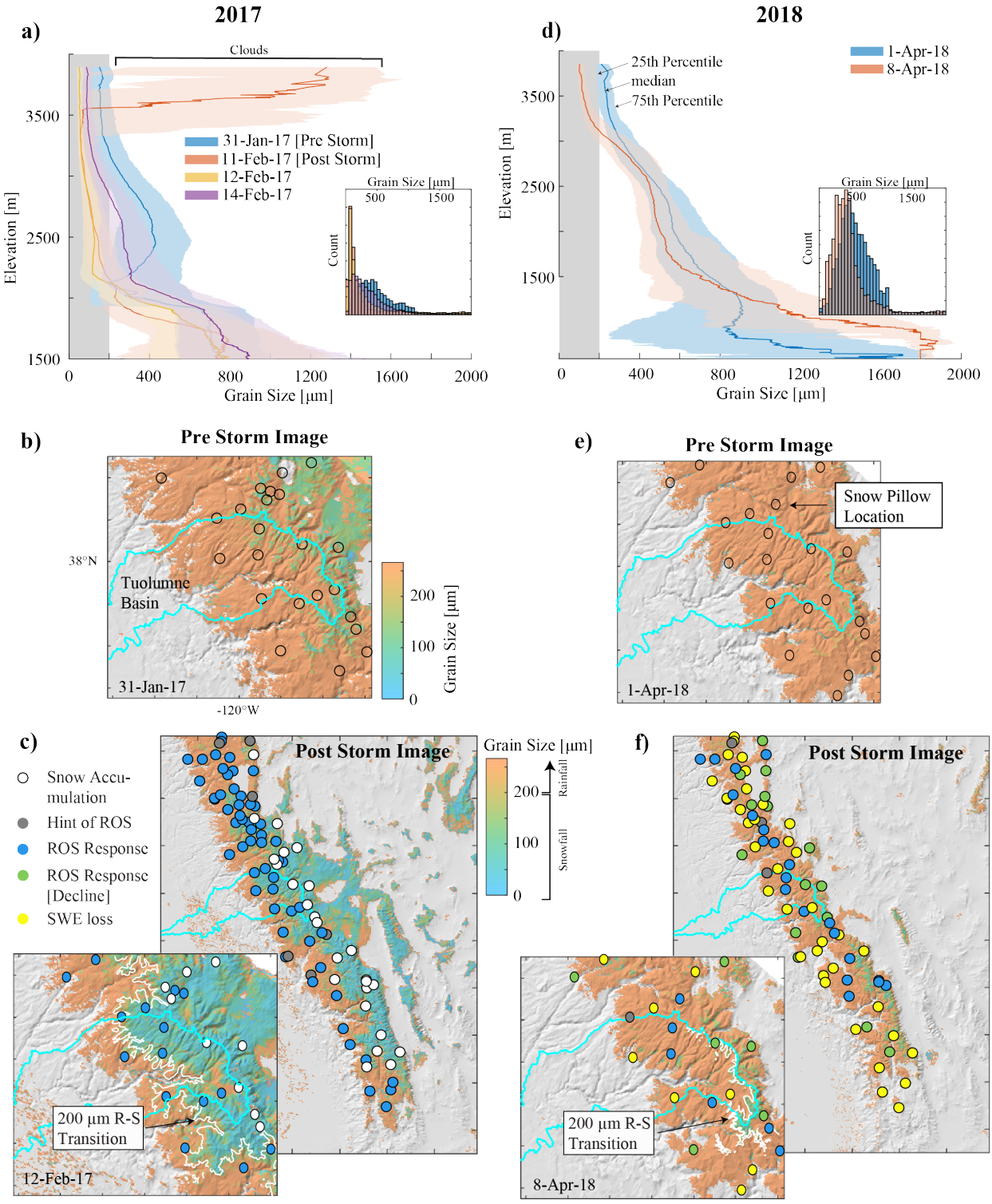
2017
a)
Clouds
31-Jan-17 [Pre Storm]
11-Feb-17 [Post Storm]
12-Feb-17
14-Feb-17
Grain Size [µm]
Count
Elevation [m]
Grain Size [µm]
2018
d)
25th Percentile
median
75th Percentile
1-Apr-18
8-Apr-18
b)
Pre Storm Image
Tuolumne Basin
31-Jan-17
38°N
-120°W
Grain Size [µm]
e)
Pre Storm Image
Snow Pillow Location
1-Apr-18
c)
Post Storm Image
Snow Accumulation
Hint of ROS
ROS Response
ROS Response [Decline]
SWE loss
Rainfall
Snowfall
200 µm R-S Transition
12-Feb-17
f)
Post Storm Image
200 µm R-S Transition
8-Apr-18

Figure 3. MODIS observations of the snow grain size pre and post storms in 2017 (a, b, and c) and 2018 (d, e, and f). Snowfall drives a reduction in grain size above the R-S transition when comparing the before (blue), and after (red) elevation profiles for the Tuolumne basin ((a) and (d)). Histograms of the grain size (insets for (a) and (d)), also show the shift in grain size to smaller sizes—but not across all grain sizes (due to ROS). Images (b) and (e) show the before storm MODSCAG grain size with snow pillow locations. Images (c) and (f) show the post grain sizes for the Sierra Nevada and the Tuolumne (inset maps) along with snow pillow ROS responses. During the 2018 storm (f), traces of snowfall were only present at the very highest elevations of the basin—above the snow pillow network.

5 Conclusions

We presented evidence that snow pillows "respond" during heavy rainfall and that the response can be used to map the rain-snow (R-S) transition elevation. We also showed the response can be identified during both the accumulation and ablation seasons. The response matches auxiliary observations from FMCW radars, streamflow, and when available—soil moisture sensors. Although beyond the scope of the paper, the perturbation type (i.e., pulse, collapse, and decline), and the size of the ROS response likely reflects a combination of rainfall totals, the snow energy balance, snowpack antecedent conditions, and in some cases, local snow pillow placement. Finally, we have also shown how remote sensing of the snow grain size can be used to detect the end-of-storm R-S transition if rain-on-snow occurs. We found that the 200 m grain size elevation represents the R-S transition and aligns well with FMCW radars (within 100 m). These observations and insights support validation needs for improving the meteorological models that are used in operational precipitation and streamflow forecasting. Continued efforts to leverage existing technology in novel ways are essential to enhancing California's water supply reliability and mitigating flood hazard in a timely and cost-effective manner.

Acknowledgments, Samples, and Data

The authors declare no real or perceived conflict of interest. Work was conducted under UCAR Subaward 001987, and while all data are public the data used herein are housed in a fair compliant repository: (https://doi.org/10.5281/zenodo.5998949). Lastly, we would like to thank California DWR's Hydrology Branch for their group's time and insight on snow pillow practices.

References

https://doi.org/10.3389/feart.2021.617594

https://doi.org/10.1029/2019WR024828

https://doi.org/10.1029/2019WR025331

https://doi.org/10.1029/2012GL051736

https://doi.org/10.1016/0021-9797(79)90340-0

https://doi.org/10.1029/93WR03247
https://doi.org/10.1016/j.advwatres.2008.08.011
https://doi.org/10.1016/j.rse.2007.07.029
https://doi.org/10.1016/j.jhydrol.2017.01.051
https://doi.org/10.1002/hyp.9666
https://doi.org/10.1002/2016GL067978
https://doi.org/10.5194/hess-21-1-2017
https://doi.org/10.3390/atmos9060233
https://doi.org/10.3390/w9110899
https://doi.org/10.1029/2020EA001129
https://doi.org/10.1029/2012GL053866
https://doi.org/10.1029/2020GL088189
https://doi.org/10.1175/jhm-d-18-0212.1
https://doi.org/10.1029/2011RG000365
https://doi.org/10.1002/2016EF000514
https://doi.org/10.1002/hyp.5795
https://doi.org/10.5194/hess-21-4973-2017
https://doi.org/10.3189/1985AoG6-1-272-273
https://doi.org/10.3189/S0260305500007758
https://doi.org/10.5194/hess-18-4261-2014
https://doi.org/10.1175/JCLI3850.1
https://doi.org/10.1029/2019WR024950
https://doi.org/10.5194/hess-24-5317-2020
https://doi.org/10.1002/(SICI)1099-1085(199808/09)12:10/11
https://doi.org/10.3189/172756401781819751
https://doi.org/10.1016/j.jhydrol.2007.12.027
https://doi.org/10.1175/JAS-D-12-0194.1
https://doi.org/10.1175/jhm-d-12-035.1
https://doi.org/10.1038/s41612-018-0012-1
https://doi.org/10.1038/s41558-018-0236-4
https://doi.org/10.1016/j.rse.2009.01.001

https://doi.org/10.1016/j.rse.2016.06.018

https://doi.org/10.1002/hyp.10905

https://doi.org/10.1038/s41558-020-0825-x

http://doi.org/10.1175/1520-0493(2004)132

https://doi.org/10.1007/978-3-030-28906-5

https://doi.org/10.1146/annurev.earth.33.092203.122541

https://doi.org/10.5194/hess-18-2265-2014

https://doi.org/10.1038/s43017-021-00219-y

https://doi.org/10.1016/S0022-1694(97)00004-8

https://doi.org/10.1029/2020WR027072

https://doi.org/10.1002/2014WR016576

https://doi.org/10.1175/BAMS-D-18-0091.1

https://doi.org/10.1175/2009jhm1181.1

https://doi.org/10.1175/jtech-d-12-00217.1

https://doi.org/10.1175/jhm-d-15-0181.1

Arienzo, M. M., M. Collins, and K. S. Jennings (2021), Enhancing engagement of citizen scientists to monitor precipitation phase, *Frontiers in Earth Science*, *9*(68). Avanzi, F., R. C. Johnson, C. A. Oroza, H. Hirashima, T. Maurer, and S. Yamaguchi (2019), Insights Into Preferential Flow Snowpack Runoff Using Random Forest, *Water Resources Research*, *55*(12), 10727-10746. Brandt, W. T., K. J. Bormann, F. Cannon, J. S. Deems, T. H. Painter, D. F. Steinhoff, and J. Dozier (2020), Quantifying the spatial variability of a snowstorm using differential airborne lidar, *Water Resources Research*, *56*(3), e2019WR025331. Catto, J. L., C. Jakob, G. Berry, and N. Nicholls (2012), Relating global precipitation to atmospheric fronts, *Geophysical Research Letters*, *39*(10). Colbeck, S. C. (1979), Grain clusters in wet snow, *Journal of Colloid and Interface Science*, *72*(3), 371-384. Conway, H., and R. Benedict (1994), Infiltration of water into snow, *Water Resources Research*, *30*(3), 641-649. Dozier, J., T. H. Painter, K. Rittger, and J. E. Frew (2008), Time–space continuity of daily maps of fractional snow cover and albedo from MODIS, *Advances in Water Resources*, *31*(11), 1515-1526. Dozier, J., R. O. Green, A. W. Nolin, and T. H. Painter (2009), Interpretation of snow properties from imaging spectrometry, *Remote Sensing of Environment*, *113*, S25-S37. Dudley, R. W., G. A. Hodgkins, M. R. McHale, M. J. Kolian, and B. Renard (2017), Trends in snowmelt-related streamflow timing in the conterminous United States, *Journal of Hydrology*, *547*, 208-221. Eiriksson, D., M. Whitson, C. H. Luce, H. P. Marshall, J. Bradford, S. G. Benner, T. Black, H. Hetrick, and J. P. McNamara (2013), An evaluation of the hydrologic relevance of lateral flow in snow at hillslope and catchment scales, *Hydrological Processes*,

27(5), 640-654. Guan, B., D. E. Waliser, F. M. Ralph, E. J. Fetzer, and P. J. Neiman (2016), Hydrometeorological characteristics of rain-on-snow events associated with atmospheric rivers, *Geophysical Research Letters*, *43*(6), 2964-2973. Harpold, A. A., M. L. Kaplan, P. Z. Klos, T. Link, J. P. McNamara, S. Rajagopal, R. Schumer, and C. M. Steele (2017), Rain or snow: hydrologic processes, observations, prediction, and research needs, *Hydrol. Earth Syst. Sci.*, *21*(1), 1-22. Hatchett, B. J. (2018), Snow level characteristics and impacts of a spring typhoon-originating atmospheric river in the Sierra Nevada, USA, *Atmosphere*, *9*(6), 233. Hatchett, B. J., B. Daudert, C. B. Garner, N. S. Oakley, A. E. Putnam, and A. B. White (2017), Winter snow level rise in the northern Sierra Nevada from 2008 to 2017, *Water*, *9*(11), 899. Hatchett, B. J., et al. (2020), Observations of an extreme atmospheric river storm with a diverse sensor network, *Earth and Space Science*, *7*(8), e2020EA001129. Hawcroft, M. K., L. C. Shaffrey, K. I. Hodges, and H. F. Dacre (2012), How much Northern Hemisphere precipitation is associated with extratropical cyclones?, *Geophysical Research Letters*, *39*(24). Henn, B., K. N. Musselman, L. Lestak, F. M. Ralph, and N. P. Molotch (2020a), Extreme runoff generation from atmospheric river driven snowmelt during the 2017 Oroville Dam spillways incident, *Geophysical Research Letters*, *47*(14), e2020GL088189. Henn, B., R. Weihs, A. C. Martin, F. M. Ralph, and T. Osborne (2020b), Skill of rain-snow level forecasts for landfalling atmospheric rivers: a multimodel assessment using California's network of vertically profiling radars, *Journal of Hydrometeorology*, *21*(4), 751-771. Houze, R. A. (2012), Orographic effects on precipitating clouds, *Reviews of Geophysics*, *50*(1), RG1001. Huss, M., et al. (2017), Toward mountains without permanent snow and ice, *Earth's Future*, *5*(5), 418-435. Johnson, J. B., and D. Marks (2004), The detection and correction of snow water equivalent pressure sensor errors, *Hydrological Processes*, *18*(18), 3513-3525. Juras, R., S. Würzer, J. Pavlásek, T. Vitvar, and T. Jonas (2017), Rainwater propagation through snowpack during rain-on-snow sprinkling experiments under different snow conditions, *Hydrol. Earth Syst. Sci.*, *21*(9), 4973-4987. Kattelmann, R. (1985), Macropores in snowpacks of Sierra Nevada, *Annals of Glaciology*, *6*, 272-273. Kattelmann, R. (1987), Water release from a forested snowpack during rainfall, *Forest Hydrology and Watershed Management*, *167*, 265-272. Kattelmann, R. (1989), Spatial variability of snowpack outflow at a site in Sierra Nevada, U.S.A, *Annals of Glaciology*, *13*, 124-128. Kattelmann, R. (1997), Flooding from rain-on-snow events in the Sierra Nevada, *IAHS Publications-Series of Proceedings and Reports-Intern Assoc Hydrological Sciences*, *239*, 59-66. Kirchner, P. B., R. C. Bales, N. P. Molotch, J. Flanagan, and Q. Guo (2014), LiDAR measurement of seasonal snow accumulation along an elevation gradient in the southern Sierra Nevada, California, *Hydrology and Earth System Sciences*, *18*(10), 4261-4275. Knowles, N., M. D. Dettinger, and D. R. Cayan (2006), Trends in snowfall versus rainfall in the Western United States, *Journal of Climate*, *19*(18), 4545-4559. Li, D., D. P. Lettenmaier, S. A. Margulis, and K. Andreadis (2019), The role of rain-on-snow in flooding over the conterminous United States, *Water Resources Research*, *55*(11), 8492-8513. Lynn, E., A. Cuthbertson, M. He, J. P. Vasquez, M. L. Anderson, P. Coombe, J. T. Abatzoglou, and B. J. Hatch-

ett (2020), Technical note: precipitation-phase partitioning at landscape scales to regional scales, *Hydrol. Earth Syst. Sci.*, *24*(11), 5317-5328. Marks, D., J. Kimball, D. Tingey, and T. Link (1998), The sensitivity of snowmelt processes to climate conditions and forest cover during rain-on-snow: a case study of the 1996 Pacific Northwest flood, *Hydrological Processes*, *12*(10-11), 1569-1587. <1569::AID-HYP682>3.0.CO;2-LMarks, D., T. Link, A. Winstral, and D. Garen (2001), Simulating snowmelt processes during rain-on-snow over a semi-arid mountain basin, *Annals of Glaciology*, *32*, 195-202. Mazurkiewicz, A. B., D. G. Callery, and J. J. McDonnell (2008), Assessing the controls of the snow energy balance and water available for runoff in a rain-on-snow environment, *Journal of Hydrology*, *354*(1), 1-14. McGurk, B. J., and P. Marsh (1995), Flow-finger continuity in serial thick-sections in a melting Sierran snowpack, in *Biogeochemistry of Seasonally Snow-Covered Catchments*, edited by K. A. Tonnessen, M. W. Williams and M. Tranter, pp. 81-88, Int Assoc Hydrological Sciences, Wallingford.Minder, J. R., and D. E. Kingsmill (2013), Mesoscale variations of the atmospheric snow line over the northern Sierra Nevada: multiyear statistics, case study, and mechanisms, *Journal of the Atmospheric Sciences*, *70*(3), 916-938. Mizukami, N., V. Koren, M. Smith, D. Kingsmill, Z. Zhang, B. Cosgrove, and Z. Cui (2013), The impact of precipitation type discrimination on hydrologic simulation: rain-snow partitioning derived from HMT-West radar-detected brightband height versus surface temperature data, *Journal of Hydrometeorology*, *14*(4), 1139-1158. Mote, P. W., S. Li, D. P. Lettenmaier, M. Xiao, and R. Engel (2018), Dramatic declines in snowpack in the western US, *npj Climate and Atmospheric Science*, *1*(1), 2. Musselman, K. N., F. Lehner, K. Ikeda, M. P. Clark, A. F. Prein, C. Liu, M. Barlage, and R. Rasmussen (2018), Projected increases and shifts in rain-on-snow flood risk over western North America, *Nature Climate Change*, *8*(9), 808-812. Painter, T. H., K. Rittger, C. McKenzie, P. Slaughter, R. E. Davis, and J. Dozier (2009), Retrieval of subpixel snow covered area, grain size, and albedo from MODIS, *Remote Sensing of Environment*, *113*(4), 868-879. Painter, T. H., et al. (2016), The Airborne Snow Observatory: Fusion of scanning lidar, imaging spectrometer, and physically-based modeling for mapping snow water equivalent and snow albedo, *Remote Sensing of Environment*, *184*, 139-152. Pomeroy, J. W., X. Fang, and D. G. Marks (2016), The cold rain-on-snow event of June 2013 in the Canadian Rockies — characteristics and diagnosis, *Hydrological Processes*, *30*(17), 2899-2914. Prein, A. F., and A. J. Heymsfield (2020), Increased melting level height impacts surface precipitation phase and intensity, *Nature Climate Change*, *10*(8), 771-776. Ralph, F. M., P. J. Neiman, and G. A. Wick (2004), Satellite and CALJET aircraft observations of atmospheric rivers over the eastern north Pacific Ocean during the winter of 1997/98, *Monthly Weather Review*, *132*(7), 1721-1745. <1721:Sacaoo>2.0.Co;2Ralph, F. M., M. D. Dettinger, J. J. RutzDuane, and E. Waliser (2020), *Atmospheric Rivers*, Springer. .Roe, G. H. (2005), Orographic precipitation, *Annual Review of Earth and Planetary Sciences*, *33*(1), 645-671. Rössler, O., P. Froidevaux, U. Börst, R. Rickli, O. Martius, and R. Weingartner (2014), Retrospective analysis of a nonforecasted rain-on-snow flood in the Alps – a matter of model limitations or unpredictable

nature?, *Hydrol. Earth Syst. Sci.*, *18*(6), 2265-2285. Siirila-Woodburn, E. R., et al. (2021), A low-to-no snow future and its impacts on water resources in the western United States, *Nature Reviews Earth & Environment*, *2*(11), 800-819. Singh, P., G. Spitzbart, H. Hübl, and H. W. Weinmeister (1997), Hydrological response of snowpack under rain-on-snow events: a field study, *Journal of Hydrology*, *202*(1), 1-20. Sumargo, E., F. Cannon, F. M. Ralph, and B. Henn (2020), Freezing level forecast error can consume reservoir flood control storage: potentials for Lake Oroville and New Bullards Bar reservoirs in California, *Water Resources Research*, *56*(8), e2020WR027072. Wayand, N. E., J. D. Lundquist, and M. P. Clark (2015), Modeling the influence of hypsometry, vegetation, and storm energy on snowmelt contributions to basins during rain-on-snow floods, *Water Resources Research*, *51*(10), 8551-8569. White, A. B., B. J. Moore, D. J. Gottas, and P. J. Neiman (2019), Winter storm conditions leading to excessive runoff above California's Oroville Dam during January and February 2017, *Bulletin of the American Meteorological Society*, *100*(1), 55-70. White, A. B., D. J. Gottas, A. F. Henkel, P. J. Neiman, F. M. Ralph, and S. I. Gutman (2010), Developing a performance measure for snow-level forecasts, *Journal of Hydrometeorology*, *11*(3), 739-753. White, A. B., et al. (2013), A twenty-first-century California observing network for monitoring extreme weather events, *Journal of Atmospheric and Oceanic Technology*, *30*(8), 1585-1603. Würzer, S., T. Jonas, N. Wever, and M. Lehning (2016), Influence of initial snowpack properties on runoff formation during rain-on-snow events, *Journal of Hydrometeorology*, *17*(6), 1801-1815.